Experimental and theoretical study of longitudinal power distribution in a random DFB fiber laser

Dmitry V. Churkin,[1,2,3,*] Atalla E. El-Taher,[3] Ilya D. Vatnik,[1,2] Juan Diego Ania-Castañón,[4] Paul Harper,[3] Eugeny V. Podivilov,[1] Sergey A. Babin,[1] and Sergei K. Turitsyn[3]

[1]*Institute of Automation and Electrometry SB RAS, 1 Ac. Koptyug ave., Novosibirsk, 630090, Russia*
[2]*Novosibirsk State University, 2 Pirogova str., Novosibirsk, 630090, Russia*
[3]*Aston Institute of Photonic Technologies, Aston University, Birmingham, B4 7ET, UK*
[4]*Instituto de Óptica "Daza de Valdés", IO-CSIC, CSIC, Madrid, 28006, Spain*
[*]*d.churkin@aston.ac.uk*

Abstract: We have measured the longitudinal power distribution inside a random distributed feedback Raman fiber laser. The observed distribution has a sharp maximum whose position depends on pump power. The spatial distribution profiles are different for the first and the second Stokes waves. Both analytic solution and results of direct numerical modeling are in excellent agreement with experimental observations.

OCIS codes: (140.3510) Lasers, fiber; (140.3490) Lasers, distributed-feedback; (290.5910) Scattering, stimulated Raman; (290.5870) Scattering, Rayleigh.

References and links

1. S. K. Turitsyn, S. A. Babin, A. E. El-Taher, P. Harper, D. V. Churkin, S. I. Kablukov, J. D. Ania-Castañón, V. Karalekas, and E. V. Podivilov, "Random distributed feedback fibre laser," Nat. Photonics **4**(4), 231–235 (2010).
2. H. Cao, "Review on latest developments in random lasers with coherent feedback," J. Phys. A **38**(49), 10497–10535 (2005).
3. D. S. Wiersma, "The physics and applications of random lasers," Nat. Phys. **4**(5), 359–367 (2008).
4. J. Fallert, R. Dietz, J. Sartor, D. Schneider, C. Klingshirn, and H. Kalt, "Co-existence of strongly and weakly localized random laser modes," Nat. Photonics **3**(5), 279–282 (2009).
5. M. Leonetti, C. Conti, and C. Lopez, "The mode-locking transition of random lasers," Nat. Photonics **5**(10), 615–617 (2011).
6. D. V. Churkin, S. A. Babin, A. E. El-Taher, P. Harper, S. I. Kablukov, V. Karalekas, J. D. Ania-Castanon, E. V. Podivilov, and S. K. Turitsyn, "Raman fiber lasers with a random distributed feedback based on Rayleigh scattering," Phys. Rev. A **82**(3), 033828 (2010).
7. A. M. R. Pinto, M. Bravo, M. Fernandez-Vallejo, M. Lopez-Amo, J. Kobelke, and K. Schuster, "Suspended-core fiber Sagnac combined dual-random mirror Raman fiber laser," Opt. Express **19**(12), 11906–11915 (2011).
8. A. R. Sarmani, M. H. Abu Bakar, A. A. Bakar, F. R. Adikan, and M. A. Mahdi, "Spectral variations of the output spectrum in a random distributed feedback Raman fiber laser," Opt. Express **19**(15), 14152–14159 (2011).
9. I. D. Vatnik, D. V. Churkin, S. A. Babin, and S. K. Turitsyn, "Cascaded random distributed feedback Raman fiber laser operating at 1.2 μm," Opt. Express **19**(19), 18486–18494 (2011).
10. A. M. R. Pinto, O. Frazão, J. L. Santos, and M. Lopez-Amo, "Multiwavelength fiber laser based on a photonic crystal fiber loop mirror with cooperative Rayleigh scattering," Appl. Phys. B **99**(3), 391–395 (2010).
11. A. E. El-Taher, P. Harper, S. A. Babin, D. V. Churkin, E. V. Podivilov, J. D. Ania-Castanon, and S. K. Turitsyn, "Effect of Rayleigh-scattering distributed feedback on multiwavelength Raman fiber laser generation," Opt. Lett. **36**(2), 130–132 (2011).
12. S. A. Babin, A. E. El-Taher, P. Harper, E. V. Podivilov, and S. K. Turitsyn, "Tunable random fiber laser," Phys. Rev. A **84**(2), 021805(R) (2011).
13. S. K. Turitsyn, J. D. Ania-Castañón, S. A. Babin, V. Karalekas, P. Harper, D. Churkin, S. I. Kablukov, A. E. El-Taher, E. V. Podivilov, and V. K. Mezentsev, "270-km ultralong Raman fiber laser," Phys. Rev. Lett. **103**(13), 133901 (2009).
14. J. D. Ania-Castañón, T. J. Ellingham, R. Ibbotson, X. Chen, L. Zhang, and S. K. Turitsyn, "Ultralong Raman fiber lasers as virtually lossless optical media," Phys. Rev. Lett. **96**(2), 023902 (2006).
15. S. A. Babin, D. V. Churkin, and E. V. Podivilov, "Intensity interactions in cascades of a two-stage Raman fiber laser," Opt. Commun. **226**(1-6), 329–335 (2003).

#162353 - $15.00 USD
Received 1 Feb 2012; accepted 24 Feb 2012; published 1 May 2012

16. S. A. Babin, V. Karalekas, E. V. Podivilov, V. K. Mezentsev, P. Harper, J. D. Ania-Castañón, and S. K. Turitsyn, "Turbulent broadening of optical spectra in ultralong Raman fiber lasers," Phys. Rev. A **77**(3), 033803 (2008).
17. S. A. Babin, D. V. Churkin, A. E. Ismagulov, S. I. Kablukov, and E. V. Podivilov, "Four-wave-mixing-induced turbulent spectral broadening in a long Raman fiber laser," J. Opt. Soc. Am. B **24**(8), 1729–1738 (2007).
18. S. A. Babin, V. Karalekas, P. Harper, E. V. Podivilov, V. K. Mezentsev, J. D. Ania-Castañón, and S. K. Turitsyn, "Experimental demonstration of mode structure in ultralong Raman fiber lasers," Opt. Lett. **32**(9), 1135–1137 (2007).
19. D. B. Soh, J. P. Koplow, S. W. Moore, K. L. Schroder, and W. L. Hsu, "The effect of dispersion on spectral broadening of incoherent continuous-wave light in optical fibers," Opt. Express **18**(21), 22393–22405 (2010).
20. J. D. Ania-Castañón, "Quasi-lossless transmission using second-order Raman amplification and fibre Bragg gratings," Opt. Express **12**(19), 4372–4377 (2004).
21. S. Foster and A. Tikhomirov, "Experimental and theoretical characterization of the mode profile of single-mode DFB fiber lasers," IEEE J. Quantum Electron. **41**(6), 762–766 (2005).
22. N. Lizárraga, N. P. Puente, E. I. Chaikina, T. A. Leskova, and E. R. Méndez, "Single-mode Er-doped fiber random laser with distributed Bragg grating feedback," Opt. Express **17**(2), 395–404 (2009).
23. M. Gagné and R. Kashyap, "Demonstration of a 3 mW threshold Er-doped random fiber laser based on a unique fiber Bragg grating," Opt. Express **17**(21), 19067–19074 (2009).

1. Introduction

Recently, the novel concept of a fiber laser operating via the feedback produced by randomly distributed variations of refractive index in the fiber core was proposed and implemented [1]. The distributed feedback (DFB) results from the Rayleigh backscattered radiation, which is captured by the fiber waveguide and amplified through the Raman effect. The lasing mechanism in such random DFB fiber laser is similar to the one seen in random lasers where light is generated in an amplifying disordered medium without a traditional cavity (see [2–5] for a review). Still, random DFB Raman fiber lasers when compared to traditional random lasers present important differences arising from the feedback mechanism: Weak and continuous Rayleigh scattering (RS) in a fiber, in opposition to the strong discrete reflections in other random lasers, leads to a rather different geometry (very long 1-dimentional random medium) as well as to unique output characteristics (stable narrow-line high-quality beam).

Different fiber laser systems based on the random DFB concept were studied in the past year [6–8] demonstrating output characteristics at telecommunications transparency window (~1.55 μm) comparable to those of conventional Raman fiber lasers, as well as the possibility of short-wavelength operation (<1.2 μm), involving the first- and the second-order Stokes waves [9]. Moreover, multi-wavelength [10, 11] and widely tunable [12] random DFB fiber lasers have also been demonstrated which in some cases surprisingly outperform conventional Raman fiber lasers. A simple model has been proposed [12] that explains this fact and specifically, the higher efficiency of the random DFB fiber laser and flatter tuning (power versus wavelength) curve. Since its output power is defined by the specific longitudinal distribution of the generated power along the fiber, further optimization is possible while taking into account the shape of the distribution. Another important issue is that the random DFB laser has no limit in length in contrast to ultra-long Raman fiber lasers with conventional cavity of point-action reflectors, namely fiber Bragg gratings (FBGs) [13]. This feature provides new possibilities for optical fiber communications enabling quasi-lossless data transmission [14]. Potentially, ultra-long random DFB fiber lasers could be longer than conventional ultra-long Raman fiber lasers thus enabling quasi-lossless transmission over greater distances. For such telecommunication applications, the study of longitudinal distribution of generated power is one of the key issues.

We present here measurement, numerical simulations and analytical description of the longitudinal power distribution in ultra-long random DFB fiber laser.

2. Experimental setup

We experimentally study the symmetrical configuration proposed in [1], Fig. 1. The two 1.455 μm pump lasers with maximum power up to 4 W each are coupled into the center of an 84-km span of standard telecommunication fiber SMF-28. For pump power above ~0.8 W

#162353 - $15.00 USD Received 1 Feb 2012; accepted 24 Feb 2012; published 1 May 2012

(for each pump laser), the setup starts to generate radiation at ~1.56 μm in both directions due to the Raman gain and random distributed feedback provided by the Rayleigh scattering (RS), see [1] for details.

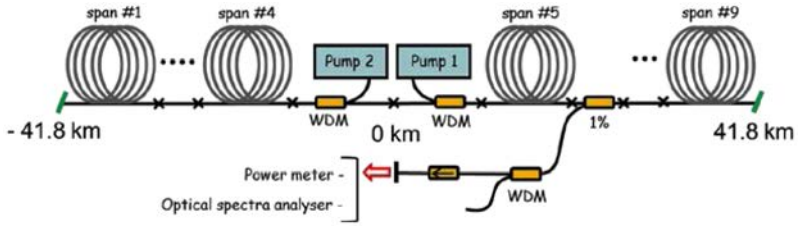

Fig. 1. The experimental setup

To measure the longitudinal distribution we use the following method. The cavity of the random DFB fiber laser has been made of 9 pieces of fiber of different lengths. All the fiber spans are spliced together to eliminate the parasitic back-reflections from the connectors which are likely to be higher than specified values of –60 dB because of high power operation and possible imperfections. A 99:1 coupler is moved through each splice point to measure both spectrum and power. The coupler is accompanied by the WDM 1455/1550 splitter eliminating the pump light and isolators to reduce the parasitic back-reflection. The coupler/WDM/isolator ("measuring unit") has been carefully calibrated at pump and generation wavelengths at different power levels. We have specially checked that the measuring unit does not affect the laser generation. It could be spliced into the cavity at splice points in two opposite directions making possible to measure independently powers of two waves travelling from left to right (so called "right wave" further) and from right to left ("left wave").

The lengths of fiber spools have been chosen in such a way that the total lengths of left and right arms, see Fig. 1, are identical, 41 km 843 meters. The chosen lengths of the fiber spools allow one to measure the generated power at the following points along the cavity: z = –41,8 km (left output), –35.2 km, –28.6 km, –21.9 km, 0 km (pump coupling point), 6.6 km, 11.5 km, 22.5 km, 31.7 km and 41.8 km (right output). We expect that in the symmetric configuration under study, the longitudinal distribution should be also symmetric relative to the pump coupling point, z = 0 (see, for example, preliminary calculations of the longitudinal distribution in [1]). Taking into account the differences in individual span lengths in opposite arms, the number of points in the longitudinal distribution of the generated wave can be almost doubled using the symmetry of the scheme. Note that we have specially designed the fiber cavity in such a way to have a symmetry checking point inside the cavity. Indeed, all our measurements at close distances (–21.9 km and 22.5 km) are nearly identical.

At each measurement point, we have measured the generated power for counter-propagating waves using a power meter and the optical spectra for different spectral components through an optical spectrum analyzer.

3. Experimental results

Firstly, together with the usual plot of output laser power, one can now plot the dependence of the generated power on the pump power at a specific point inside the cavity, Fig. 2. Above the threshold pump power (~0.8 W for each pump laser), the first Stokes wave power (~1.56 μm) grows nearly linearly. For pump power above ~2 W (for each pump laser), the second Stokes wave (~1.68 μm) is generated similar to the cascaded generation observed in random DFB fiber laser operating in the 1.2 μm spectral band [9]. Above the generation threshold of the second Stokes wave, the output power of the first Stokes wave stops growing, Fig. 2 (z = 22 km and z = 42 km), because of its conversion into the second Stokes wave, similarly to what happens in a Raman fiber laser with a FBG-based high-Q cavity, see [15] and citations

#162353 - $15.00 USD Received 1 Feb 2012; accepted 24 Feb 2012; published 1 May 2012

therein. Note that the specific character of the first Stokes output power depletion is quite different: it is not just saturating at constant level (or slightly growing) like in conventional Raman laser [15], but is decreasing rapidly down to zero.

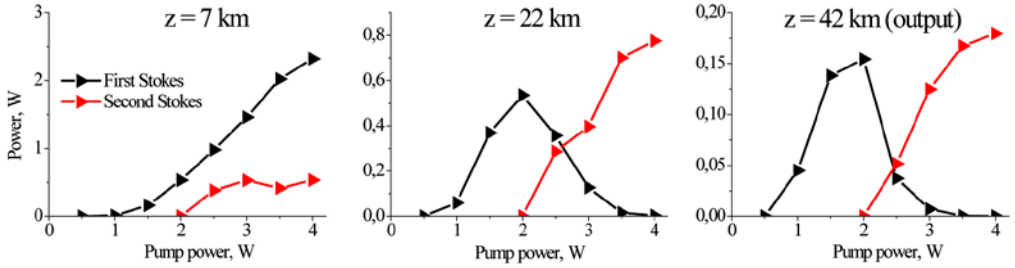

Fig. 2. The generated power for the right travelling wave at the different points along the fiber. At the X axis the power of only one pump is indicated. The total pump power coupled to the cavity is 2 times higher.

The full longitudinal distributions of the generated first Stokes wave power at different pump powers are plotted in Fig. 3(a). The power distributions for opposite (left and right) travelling waves are symmetric: both waves increase rapidly after passing the pump coupling point (z = 0), reach maximum power at some point near the middle of the fiber arm and attenuate exponentially after passing the maximum with a coefficient nearly corresponding to linear loss at 1.56 μm. The position of the power maximum along the fiber was previously found to be at the point where local value of the unsaturated Raman gain becomes equal to the loss level, $|z| = L_{RS}$, see [1] for details. In other words, $|z| = L_{RS}$ defines the boundary of a gain region. The measurements show that with increasing power the position of the power maximum shifts closer to the z = 0, and the distribution becomes correspondingly narrower.

At pump powers higher than second Stokes wave generation threshold, the power of the first Stokes attenuates at $|z|>L_{RS}$ much faster than at lower pump powers owing to the depletion process. At the highest available pump power, when the power of the second Stokes wave becomes high, see Fig. 3(b), the first Stokes wave distribution becomes very narrow, and all the generated first Stokes wave power is localized within the region |z|<10 km. At the same time, the second Stokes wave distribution is much broader with maximum located at longer distances, |z|>10 km.

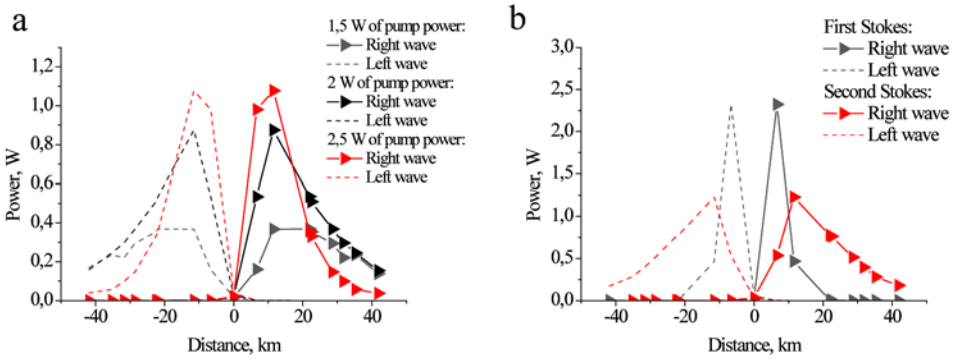

Fig. 3. (a) Longitudinal power distribution for the first Stokes wave in the center-pumped symmetrical configuration at different pump power levels (1, 2 and 2.5 W). (b) The second Stokes wave power distribution compared with the first Stokes wave power distribution at the pump power level of 4 W.

We have also carefully measured the spectra of the generated radiation at different points along the fiber. The generated spectra have the same shape at all points along the cavity, Fig. 4(a). Moreover, left and right waves measured at the same coordinate also have the same

#162353 - $15.00 USD Received 1 Feb 2012; accepted 24 Feb 2012; published 1 May 2012

spectral shape, Fig. 4(b). This fact confirms the principal role of the RS-based distributed feedback in the random fiber laser. Despite its extremely small value, the feedback couples both waves resulting in an identical spectrum for all points inside the distributed laser cavity, similar to a conventional ultra-long laser cavity (excepting in the regions near FBG reflectors) [16]. The equilibrium shape of the spectrum is nearly the same in both types of ultra-long fiber lasers (with and without FBGs): it has ~1 nm width and specific shape with exponential tails. Such shape in conventional Raman fiber lasers is formed due to the turbulent-like nonlinear interaction of multiple longitudinal modes in linear cavity [17, 18], but in the studied random DFB laser of the same length as in [18] there are no discrete cavity modes, so the spectrum consists of a continuum of random frequencies. Nevertheless, the spectral shape is similar. Note that the light propagating in a fiber exhibits substantial spectrum changes during its propagation [19], however some stationary spectrum could also set up after long-distance propagation because of the interplay between nonlinearity and dispersion.

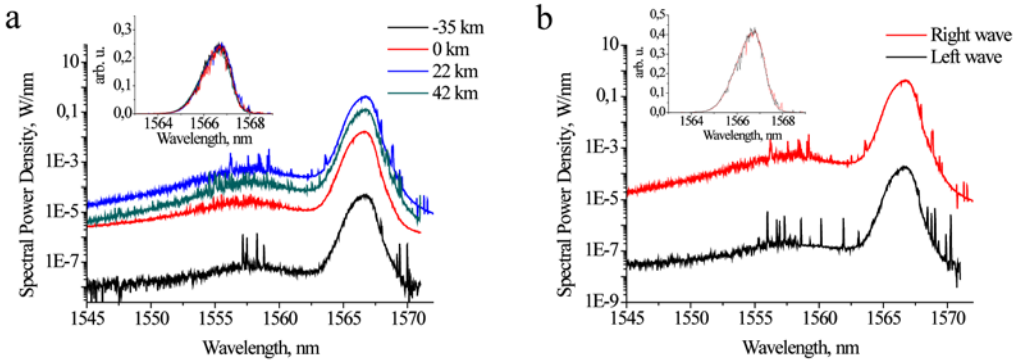

Fig. 4. (a) Spectra of right wave at specific pump power of 2 W at different points of the fiber span. (b) Right and left waves spectra at 22 km point, having the same shape. The normalized spectra in linear scale are shown in insets.

4. Numerical calculation of the power distribution

The experimentally measured distributions have been compared to theoretical predictions. To calculate numerically the longitudinal power distributions, we use the well-known power balance equation model [20]:

$$\begin{cases} (\alpha_P \pm d/dz)P_P^{\pm} = -g_S P_P^{\pm}(P_S^{+} + P_S^{-} + 4h\nu_S\Delta\nu)\dfrac{\nu_P}{\nu_S} + \varepsilon_P \cdot P_P^{\mp} \\ (\alpha_S \pm d/dz)P_S^{\pm} = g_S P_P^{+}(P_S^{\pm} + 2h\nu_S\Delta\nu) + \varepsilon_S \cdot P_S^{\mp} - g_{2S} P_S^{\pm}(P_{2S}^{+} + P_{2S}^{-} + 4h\nu_{2S}\Delta\nu)\dfrac{\nu_S}{\nu_{2S}} \\ (\alpha_{2S} \pm d/dz)P_{2S}^{\pm} = g_{2S}(P_S^{+} + P_S^{-})(P_{2S}^{\pm} + 2h\nu_{2S}\Delta\nu) + \varepsilon_{2S} \cdot P_{2S}^{\mp} \end{cases} \quad (1)$$

Here lower indexes *P*, *S*, *2S* refer the corresponding terms to pump, Stokes and second Stokes waves, while upper indexes + and – refer to forward ("right") and backward ("left") propagating waves, respectively. Coefficients α define the attenuation of the corresponding wave, g is the Raman gain coefficient, ν is the radiation frequency, $\Delta\nu$ is the Raman amplification bandwidth, ε is the backscattering coefficient, derived as α multiplied by backscattering factor Q. Backscattered factor was measured in special experiments and amounts approximately to $Q \approx 10^{-3}$ for the used fiber. As the studied configuration is symmetric against reflection ($z \rightarrow -z$) with corresponding changes in upper indexes ($+ \leftrightarrow -$), we can use just the positive arm ($z>0$) in modeling, with the appropriate boundary conditions:

#162353 - $15.00 USD Received 1 Feb 2012; accepted 24 Feb 2012; published 1 May 2012

$$\begin{cases} P_S^+(0) = P_S^-(0)(1-\chi), \quad P_{2S}^+(0) = P_{2S}^-(0)(1-\chi) \\ P_S^-(L) = P_{2S}^-(L) = P_P^-(L) = 0 \end{cases} \tag{2}$$

Here χ is the fractional loss due to splices, connectors etc., between the two arms of the laser, $L \approx 42$ km is the length of one fiber arm.

Fiber parameters used are summarized in Table 1.

Table 1. Parameters of the Fiber under Study

Wavelength (nm)	α, km^{-1}	g, W^{-1}km^{-1}	ε, km^{-1}
1455	0.055	0.39	$6 \cdot 10^{-5}$
1560	0.045	0.33	$4.5 \cdot 10^{-5}$
1680	0.055	-	$7 \cdot 10^{-5}$

The numerically calculated profiles for the power distribution of the first and the second Stokes waves obtained using this simple model are shown in Fig. 5 where pump power distribution is also shown for comparison (calculated just above the second threshold at 2 W for each pump unit; only right waves are shown). The calculated profiles are in qualitative agreement with the experimental ones: the position of power maximum of the second Stokes wave is shifted to longer distances compared to that for the first Stokes wave, while the pump wave is almost fully converted to the Stokes waves as confirmed by comparison to the undepleted pump wave distribution. Note that it is hardly possible to compare quantitatively the calculated and experimental results, especially for the second Stokes wave, because of the sufficient uncertainty in fiber parameters at ~1.68 μm and a lack of experimental points.

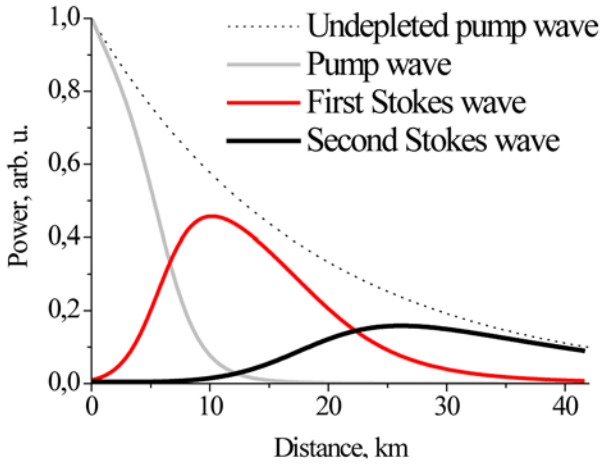

Fig. 5. Numerically calculated power distributions for the first and the second Stokes waves at 2 W pumping in comparison with pump wave distribution with (grey) and without (dashed) Stokes waves generation.

However, such a comparison seems to be possible for the first Stokes wave that demonstrates a good quantitative agreement between the experimental and theoretical distributions, calculated at pump power 2 W and neglecting the second Stokes wave, as it is seen in Fig. 6(a) (only right wave at z > 0 is shown).

#162353 - $15.00 USD
Received 1 Feb 2012; accepted 24 Feb 2012; published 1 May 2012

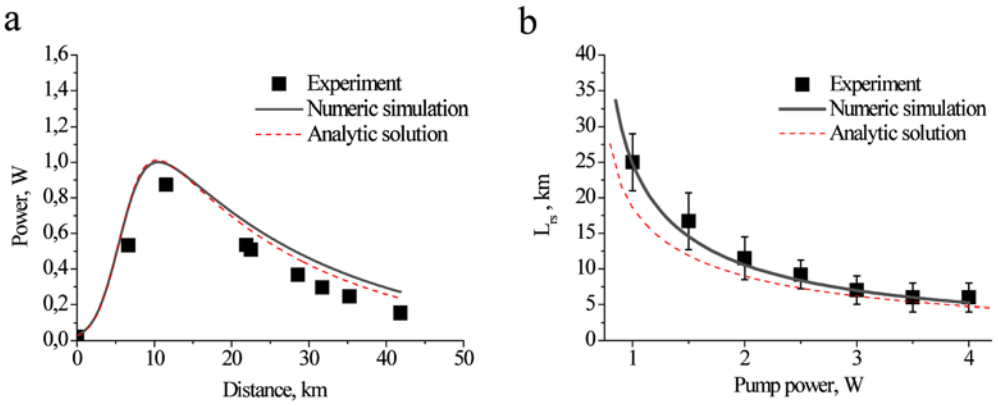

Fig. 6. Experimental, numerical and analytic results comparison: (a) longitudinal power distribution at 2 W pump power (b) L_{RS} (position of maximum) versus pump power. Analytic solution is calculated from Eqs. (9) and (17).

Apart from the longitudinal distribution, one can also calculate L_{RS} value, Fig. 6(b). At the generation threshold, L_{RS} is defined by the undepleted pump wave distribution, see Fig. 5, so the experimental value is close to the estimation L_{RS} ~ 35 km made in [1]. While pump power increases well above the threshold, the L_{RS} decreases because of the pump power depletion, see Fig. 5. The agreement between the calculated and experimental results remains reasonably good even above the generation threshold of the second Stokes wave, which distorts the first Stokes power distribution at z > L_{RS}, but not near its maximum, see Figs. 3, 5.

5. Analytical model

The symmetrical configuration under study provides a good opportunity under certain conditions to analytically find the longitudinal distribution of the generated power for the first Stokes wave, the value of the generation threshold, the dependence with the pump power of the generated power at the maximum of the distribution and its longitudinal position..

First, the following obvious condition on the forward (right) and backward (left) waves in the symmetric points should be satisfied:

$$P_S^+(z) = P_S^-(-z) \tag{3}$$

that allows us to consider again only the right arm of the scheme ($z \geq 0$).

Let us keep in the balance equation set (1) only principal terms neglecting the spontaneous emission and the second Stokes wave. In addition, we simplify the analysis assuming that linear losses α are equal for the Stokes and pump waves that is almost true when the pump and Stokes wavelength are in transmission window near 1.5 μm. Finally, we can neglect the contribution of the left wave power P_S^- to the pump power depletion, as the left wave is of two orders of magnitude smaller than the right one at positive z (see Fig. 3(a)). The resulting simplified set of equations reads as

$$\begin{cases} \dfrac{dP_S^+}{dz} = (g_S P_P^+ - \alpha) P_S^+ \\ \dfrac{dP_S^-}{dz} = -(g_S P_P^+ - \alpha) P_S^- - \varepsilon P_S^+ \\ \dfrac{dP_P^+}{dz} = -\alpha P_P^+ - g_P P_S^+ P_P^+ \end{cases} \tag{4}$$

Here $g_P = g_S \cdot \lambda_{Stokes}/\lambda_{pump}$. These equations should be solved with the following boundary conditions

#162353 - $15.00 USD Received 1 Feb 2012; accepted 24 Feb 2012; published 1 May 2012

$$\begin{cases} P_S^+(0) = P_S^-(0) \\ P_S^-(L) = 0 \end{cases} \tag{5}$$

It is straightforward to derive the following equation from (3):

$$\frac{d(P_S^+ P_S^-)}{dz} = -\varepsilon P_S^{+2} \tag{6}$$

$$P_S^2(0) \equiv P_S^+(0)P_S^-(0) = \varepsilon \int_0^L P_S^{+^2}(z)dz \tag{7}$$

Here $P_S(0)$ is the generation power of the right wave at the pump coupling point ($z = 0$). Relationship Eq. (7) defines the generation power of the right wave, $P_S(0)$ at the pump coupling point ($z = 0$) through the integral of the generation power over the fiber length.

Integrating first and third equation in Eq. (4), one can approximate the longitudinal distribution of the pump power along the fiber:

$$P_P^+(z) = P_P(0)e^{-\alpha z} \frac{g_S P_P(0) + g_P P_S(0)}{g_P P_S(0) \exp\left[(g_S P_P(0) + g_P P_S(0)) \frac{1-e^{-\alpha z}}{\alpha} \right] + g_S P_P(0)} \tag{8}$$

and, what is more interesting, the longitudinal distribution of the generated Stokes wave along the distributed cavity of the random fiber laser:

$$P_S^+(z) = P_S(0)e^{-\alpha z} \frac{g_S P_P(0) + g_P P_S(0)}{g_S P_P(0) \exp\left[-(g_S P_P(0) + g_P P_S(0)) \frac{1-e^{-\alpha z}}{\alpha} \right] + g_P P_S(0)} \tag{9}$$

Here and further $P_P(0) = P^+{}_P(0)$ is an input pump power.

To plot the longitudinal distribution $P_S^+(z)$ one needs to fit the value of the Stokes wave power $P_S(0)$ at the pump coupling point. However, the value $P_S(0)$ can also be found analytically. Indeed, to find the value of $P_S(0)$ we substitute Eq. (8) into Eq. (6):

$$1 = \varepsilon \int_0^L dz \cdot e^{-2\alpha z} \left(\frac{1 + g_P P_S(0) / g_S P_P(0)}{e^{-g_S P_P(0) \frac{1-e^{-\alpha z}}{\alpha} (1 + g_P P_S(0) / g_S P_P(0))} + g_P P_S(0) / g_S P_P(0)} \right)^2 \tag{10}$$

Assuming that $g_P P_S(0)/g_S P_P(0) << 1$, that is confirmed by the experimental data and numerical simulations (Fig. 5), we obtain

$$\frac{1}{\varepsilon} = \int_0^{L_{eff}} d\xi \frac{1 - \alpha\xi}{(e^{-g_S P_P(0)\xi} + g_P P_S(0) / g_S P_P(0))^2} \tag{11}$$

where substitution $\xi = (1 - \exp(-\alpha z))/\alpha$ is used. Here and everywhere below we assume large enough fiber lengths, $\alpha L >> 1$, such that $L_{eff} = (1 - e^{-\alpha L})/\alpha \approx 1/\alpha$.

Equation (11) can be integrated in two different limits: near and well above the generation threshold. Near the generation threshold, the generation power is almost zero, $P_S(0) = 0$. Integrating Eq. (11) in this case, one can found implicitly the generation threshold pump power P_{th}:

$$gP_{th} \exp(-gP_{th} / \alpha) \simeq \sqrt{\varepsilon\alpha / 4} \tag{12}$$

The analytically calculated value of 0.76 W is close to the measured threshold of 0.8 W.

#162353 - $15.00 USD Received 1 Feb 2012; accepted 24 Feb 2012; published 1 May 2012

Above the generation threshold Eq. (11) is integrated in polylogarithmic functions, so $P_S(0)$ could be found in principle. However, it is more insightful to derive a simple approximate solution. Indeed, within the range $g_S P_P(0)\xi < ln(g_S P_P(0)/g_P P_S(0))$ one can neglect the $g_S P_P(0)/g_P P_S(0)$ term in the denominator of the integral (11). Assuming that ξ obeys the relation $\ln(g_S P_P(0)/g_P P_S(0)) < g_S P_P(0)\xi \le g_S P_P(0)/\alpha$ one can neglect exponential term in the denominator of Eq. (11). In this case the approximate solution of Eq. (11) takes a simple analytical form and the generation power $P_S(0)$ at pump coupling point can be expressed implicitly as

$$g_P P_S(0) \simeq \sqrt{\frac{\alpha\varepsilon}{2}\left[\left(\frac{g_S P_P(0)}{\alpha} - \ln\left(\frac{g_S P_P(0)}{g_P P_S(0)}\right)\right)\left(1 + \frac{g_S P_P(0)}{\alpha} - \ln\left(\frac{g_S P_P(0)}{g_P P_S(0)}\right)\right) + \frac{1}{2}\right]} \quad (13)$$

Recall that we consider here long fiber approximation with $L_{eff} = 1/\alpha$.

At the boundary of the validity domain for Eq. (13), when $g_P P_S(0) = g_S P_P(0)\exp(-g_S P_P(0)/\alpha)$, one can define from Eq. (12) the Stokes $P_s^*(0)$ and pump $P_p^*(0)$ powers as

$$g_P P_S^*(0) = \sqrt{\alpha\varepsilon/4} \qquad g_S P_P^*(0)/\alpha = \ln\left(\frac{g_S P_P^*(0)}{\sqrt{\alpha\varepsilon/4}}\right) \quad (14)$$

The last equation exactly coincides with Eq. (12) for the threshold. Therefore, Eq. (13) works well even at the threshold pump power.

Well above the threshold, Eq. (13) can be further simplified. Using the substitution $ln(g_S P_P(0)/g_P P_S(0)) = g_S P_{th}/\alpha$, we easily derive the Stokes power at z = 0 as

$$P_S(0) = \sqrt{\frac{\varepsilon}{2\alpha}}\frac{g_S}{g_P}\left(1 - \frac{P_{th}}{P_P(0)}\right)P_P(0) \quad (15)$$

Therefore, the generation power at z = 0 exhibits linear dependence on the pump power. Comparison of the analytical solution for $Ps(0)$ Eq. (15) with numerics and the experimental data demonstrates good agreement up to certain power level, as it is seen in Fig. 7.

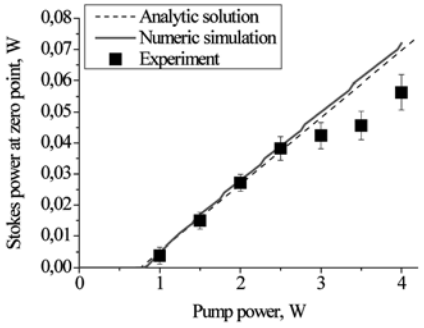

Fig. 7. Stokes right wave power at zero point (z = 0) depending on pump power.

Finally, the analytical value of $P_S(0)$ can be used in Eq. (9) to plot the longitudinal distribution of the generated power $P_S^+(z)$. There is a very good agreement between experimentally measured, analytically and numerically calculated power distributions, see Fig. 6(a).

After all, there is one more output of the developed analytical model: namely, one can find how the amplification length L_{RS} depends on pump power. Indeed, using L_{RS} definition $g_S P_P(L_{RS}) = \alpha$, it is straightforward to derive from the Eq. (8) the following equation:

$$\frac{g_S P_P(0)}{\alpha} e^{-\alpha L_{RS}} = 1 + \frac{g_P P_S(0)}{g_S P_P(0)} e^{g_S P_P(0)\left(1 - e^{-\alpha L_{RS}}\right)/\alpha} \quad (16)$$

#162353 - $15.00 USD Received 1 Feb 2012; accepted 24 Feb 2012; published 1 May 2012

While pump power increases, the amplification length decreases because of the pump power depletion. When $L_{RS} < 1/\alpha$, Eq. (16) can be simplified using Eq. (15):

$$L_{RS} = \frac{1}{g_S P_P(0)} \ln\left(g_S P_P(0) \sqrt{\frac{2}{\alpha\varepsilon}} \Big/ \left(1 - \frac{P_{th}}{P_P(0)}\right)\right) \qquad (17)$$

L_{RS} depends on pump power inversely, with the logarithmic accuracy. This analytical result is also in good agreement with both experimental data and numerical simulation, see Fig. 6(b).

6. Discussion and conclusions

Summarizing the obtained results, the longitudinal power distributions generated in the random DFB fiber laser in symmetric configuration have been studied both experimentally and theoretically. The simple analytical model describes with high accuracy first Stokes wave characteristics, namely: generation threshold, power dependence at center point (z = 0), the position of maximum power ($|z| = L_{RS}$) as well as the spatial longitudinal distribution. The numerical and analytical calculations of the first Stokes wave give very close values which are also in good quantitative agreement with obtained experimental results.

It has been found that the spectral shapes are identical for the opposite waves and do not change during the propagation of the waves along the fiber. That is consistent with the idea of Rayleigh scattering feedback being responsible for the lasing and coupling of the spectral characteristics of both waves.

The specific combination of distributed Raman amplification with maximum gain in the center (z = 0) defined by the symmetric pumping scheme and the RS-based random DFB cavity results in a specific distribution of the generated Stokes wave power. The distribution is symmetric both for the forward and backward Stokes waves, which reach maximum power at symmetric points $|z| = L_{RS}$ corresponding to the boundary of the amplification region. At $|z| > L_{RS}$ the generated power attenuates nearly exponentially with a coefficient defined by linear losses.

In previous works, the spatial mode power distribution was measured in conventional DFB fiber lasers with short (cm-long) active media in which strong regular fiber Bragg gratings with π-shift in the center was inscribed [21]. In a conventional DFB laser the generated power has maximum power at the center with exponential attenuation to fiber ends. At the absence of π-shift in a DFB cavity, power distributions for the opposite waves become different and reach their maximum values at the fiber ends corresponding to the boundary of both the active fiber and regular grating. In this sense the random DFB fiber laser has some similarity with a conventional DFB fiber laser based on a grating without phase shifts. Note that introducing irregularities in the fiber Bragg grating by means of inscription in the active fiber either an irregular array of short FBGs [22] or introducing random phase shifts in a relatively long (tens of centimeters) grating of DFB laser [23] leads to a spatial power distribution with maximum in the center of the active fiber similar to the distribution observed in a DFB fiber laser with a π-shifted regular grating [21].

Another important feature of the power distribution in the random DFB fiber laser is its dependence on the pump power. The position of maximum generated power appears to shift to the pump coupling point (z = 0) nearly inversely with pump power. Such behavior is defined by pump power depletion, see Fig. 5, leading to corresponding shift of the gain boundary point L_{RS} to the center. The model offers the way of power optimization: the half-length of the random DFB fiber laser L should be close to L_{RS} value to eliminate exponential attenuation of the generated wave thus reaching highest possible conversion efficiency (defined by loss factor $\eta \sim exp(-\alpha L)$ [12]) which could be even higher than that for conventional Raman fiber laser with linear cavity formed in the same fiber. This estimate is in agreement with the measured conversion efficiency in power maxima ($|z| = L_{RS}$), exceeding $\eta \sim 0.6$; see Fig. 3. As we have found here, increasing pump power well above the threshold

#162353 - $15.00 USD Received 1 Feb 2012; accepted 24 Feb 2012; published 1 May 2012

results in reduction of the optimal length nearly inversely with power, down to $L \sim L_{RS} < 5$ km in our case. Relevant shortening of the fiber will lead to higher random lasing threshold, however, the conversion efficiency may be further increased because of the loss reduction.

The next limitation is induced by the second Stokes wave generation after reaching the second threshold. It has been found that the second Stokes wave has quite different longitudinal distribution with maximum shifted to longer distances, $|z| > L_{RS}$. The second Stokes wave distribution is also more uniform compared to the first Stokes wave distribution at the same average generated powers. It is likely that the higher order schemes could provide an even more flat distribution that could be important for possible telecom applications such as quasi-lossless transmission [14]. Optimization of the output power for the second Stokes wave can make the optimal arm length in the symmetric scheme longer than the one for the first Stokes in correspondence with the position of maximum power for the second Stokes wave. Therefore, using the symmetric random DFB scheme one can optimize output power for each Stokes order, thus reaching maximum possible conversion efficiency of the cascaded Raman fiber laser of corresponding length for the chosen order. Note that the specific saturation character demonstrating almost full depletion of the first Stokes wave confirms high-efficiency conversion to higher order Stokes waves. Measured conversion efficiency for power values at the maxima of the distribution is over 60% not only for the first order, but also for the second order Stokes wave. In the framework of the model developed in [15] for a fiber laser with linear cavity formed by point-based mirrors, the strongly decreasing output power of the first Stokes wave at powers higher than the second Stokes wave generation threshold means strongly decreasing losses for the first Stokes wave. Indeed, the ratio of the output power to the average power inside the fiber is decreasing with pump power, Fig. 3. This may be interpreted as an increase of the finesse of the effective cavity of the random DFB fiber laser with increasing power, quite opposite to the case of a laser with a conventional FBG based cavity where a cavity finesse is decreased owing to a spectral broadening of the generated radiation in excess of the FBG bandwidth; see, e.g., [15]. Thus, this important drawback of conventional Raman fiber lasers is eliminated in the random DFB fiber laser because the distributed Rayleigh mirror is naturally broadband and has equal reflection for all frequencies inside the generated spectrum.

Thus, the obtained results have an important impact on the identification of the lasing mechanism in random DFB fiber lasers and the search for new applications.

Acknowledgments

The authors acknowledge support from the Russian Ministry of Science and Education, Russian Foundation for Basic Research, the Leverhulme Trust, the European Research Council, the Marie Curie FP7 Program IRSES, the Dynasty Foundation, Russian science support foundation, the Spanish Ministry of Science and Innovation (TEC2011-27314) and Consejo Superior de Investigaciones Científicas (2010RU0083).

#162353 - $15.00 USD Received 1 Feb 2012; accepted 24 Feb 2012; published 1 May 2012